J Solid State Electrochem (2009) 13:293–299
DOI 10.1007/s10008-008-0619-y

ORIGINAL PAPER

Spontaneous passivity of amorphous bulk Ni–Cr–Ta–Mo–Nb–P alloys in concentrated hydrochloric acids

Hiroyuki Shinomiya · Zenta Kato · Koji Hashimoto

Received: 30 September 2007 / Revised: 17 June 2008 / Accepted: 19 June 2008 / Published online: 3 August 2008

Abstract Rod-shaped amorphous bulk Ni–Cr–Mo-22 at.% Ta-14 at.%Nb–P alloys resistant to concentrated hydrochloric acids were prepared by copper-mold casting. Alloys of amorphous single phase and mixture of nanocrystalline phases in the amorphous matrix were all spontaneously passive in 6 and 12 M HCl and were immune to corrosion in 6 M HCl, although the corrosion weight loss was detected for heterogeneous alloys in 12 M HCl. Spontaneous passivation is due to presence of stable air-formed films in which chromium was particularly concentrated in addition to enrichment of tantalum and niobium. The angle resolved X-ray photoelectron spectroscopy revealed that chromium and molybdenum are rich in the inner part of the film. The major molybdenum species is in the tetravalent state, although penta- and hexavalent state molybdenum is also included. The high corrosion resistance was interpreted in terms of the high stability of the outer triple oxyhydroxide, $Cr_{1-x-y}Ta_xNb_yO_z(OH)_{3+2x+2y-2z}$, and the effective diffusion barrier of the inner Mo^{4+} and Cr^{3+} oxide layer.

Keywords Amorphous bulk alloy · Corrosion resistance in HCl · Spontaneous passivation · Roles of Cr and Mo in corrosion resistance

Contribution to the Fall Meeting of the European Materials Research Society, Symposium D: 9th International Symposium on Electrochemical/Chemical Reactivity of Metastable Materials, Warsaw, 17th-21st September, 2007.

H. Shinomiya (✉) · Z. Kato · K. Hashimoto
Tohoku Institute of Technology,
Sendai 982-8577, Japan
e-mail: shinomiya_hiroyuki@yahoo.co.jp

Introduction

Since extremely corrosion-resistant amorphous Fe–Cr–P–C alloys were found in 1974 [1], a variety of corrosion-resistant amorphous alloys have been prepared mostly by melt spinning and sputter deposition methods. In the late 1980s, Inoue, Masumoto, and their coworkers succeeded in preparing bulk amorphous magnesium [2] and indium [3] alloys by conventional casting, finding their extremely high glass-forming ability. Subsequently, the presence of the supercooled liquid state was found in some amorphous alloys [4, 5]. If the amorphous alloys show glass transition on a differential scanning calorimetry curve just below the crystallization temperature, the alloys are in the supercooled liquid state in the temperature interval between glass-transition temperature and crystallization temperature and can be processed in the desirable bulk shape in the supercooled liquid state. It was found in 1995 that even iron-based alloys became amorphous bulk rods by casting [6]. The criteria for alloys with high glass-forming ability was also proposed [7].

Recently, our effort enabled to form bulk amorphous alloy sheets resistant to concentrated hydrochloric acids by hot rolling of amorphous alloy powders in the supercooled liquid state [8]. Although preparation of amorphous alloy powder and subsequent hot rolling in the supercooled liquid state are effective in preparation of amorphous bulk alloys of desirable shape, such complicated procedure is not suitable for alloy design to form corrosion-resistant amorphous bulk alloys. By contrast, copper-mold casting is a simple method to form rod-shaped alloys, and if the cast rod of 1-mm diameter is composed of an amorphous single phase and if the alloy has the supercooled liquid state, hot

rolling of the amorphous alloy powder in the supercooled liquid state is generally effective in obtaining the amorphous bulk alloy. Thus, we are using the copper-mold casting technique for alloy design of corrosion-resistant amorphous bulk alloys.

Some of the present authors succeeded in preparing bulk amorphous Ni–15Cr–10Mo–16P [9], Ni–(10-15)Cr–5Ta–16P–4B [9], Ni-40–xNb–xTa–(3-5)P [10], Ni–Cr–Nb–P–B [11], and Ni–Cr–Ta–Mo–P–B [12] alloys by the copper-mold casting technique, which are resistant in concentrated hydrochloric acids. In particular, in Ni–Cr–Mo–22Ta–14Nb–P alloys, the addition of 1–2 at.% of both chromium and molybdenum is effective in forming alloy rods composed of the amorphous single phase and in providing the corrosion resistance in concentrated hydrochloric acids [13].

The present work is aimed to clarify the roles of the corrosion-resistant elements in enhancing the corrosion resistance in concentrated hydrochloric acids using mostly by X-ray photoelectron spectroscopy (XPS) analysis of spontaneously passivated film.

Experimental procedures

Crystalline alloy ingots were prepared by argon arc melting of commercial electrolytic nickel, electrolytic chromium, 99.9% pure molybdenum, 99.9% pure tantalum, 99.9% pure niobium, and nickel phosphide (Ni–14.17wt%P). Using these ingots, preparation of amorphous alloy rods of 1-mm diameter was tried by casting into a copper mold. For comparison, amorphous alloy ribbons of about 1-mm width and 20- to 30-μm thickness were prepared by a single roller melt-spinning method.

The structure of the thus prepared specimens was identified by X-ray diffraction with Cu Kα radiation.

Prior to immersion tests and electrochemical measurements, the surface of specimens was polished in cyclohexane with silicon carbide paper up to no. 1500, degreased in acetone and dried in air. Immersion tests and electrochemical measurements were carried out in 6 and 12 M HCl solutions open to air at 30 °C. Corrosion rates were estimated from the weight loss measured by a microbalance after immersion for 168 h. Potentiodynamic polarization curves were measured with a potential sweep rate of 5 mV s^{-1} in 6 M HCl solution open to air at 30 °C. The potential was swept from the open-circuit potential to anodic and cathodic directions using different specimens after immersion in hydrochloric acids for about 10 min. A platinum mesh and a Ag/AgCl electrode were used for counter and reference electrodes, respectively.

Before and after immersion, the surface of the specimens was analyzed by X-ray photoelectron spectroscopy. The X-ray photoelectron spectra of the specimens were measured by means of a Shimadzu ESCA-850 electron spectrometer with Mg Kα excitation (hν=1,253.6 eV). Binding energies of the photoelectrons were calibrated by a method described elsewhere [14, 15]; the binding energies of the Au $4f_{7/2}$ and $4f_{5/2}$ electrons of pure gold and the Cu $2p_{3/2}$ electrons of pure copper were taken as 84.07, 87.74, and 932.53 eV, respectively, and the kinetic energy of Cu $L_{4,5}M_{4,5}M_{4,5}$ Auger electrons of pure copper as 918.65 eV. Compositions of the surface film and the underlying alloy surface were quantitatively determined by the previously proposed method using integrated intensities of X-ray photoelectron spectra [16]. The quantitative determination was performed under the assumption of a three-layer model of the outer most contaminant hydrocarbon layer of uniform thickness, the surface film of uniform thickness, and the underlying alloy surface of X-ray photoelectron spectroscopically infinite thickness, along with the assumption of a homogeneous distribution of constituents in each layer. The photo-ionization cross-sections of Ni^{m} $2p_{3/2}$, Ni^{ox} $2p_{3/2}$, Cr $2p_{3/2}$, Mo 3d, Ta 4f, Nb 3d, and P 2p electrons relative to O 1s electrons used were 7.468 [17], 2.315 [18], 1.71 [19], 3.46 [20], 2.617 [21], 2.98 [21], and 0.786 [22], respectively. For the Ni $2p_{3/2}$ spectra, the metallic and oxidized states were distinguished and denoted by superscripts m and ox.

Results

Figure 1 shows X-ray diffraction patterns of copper-mold cast alloy rods of 1-mm diameter. The formation of alloys composed of the amorphous single phase requires the presence of both chromium and molybdenum in Ni–22Ta–

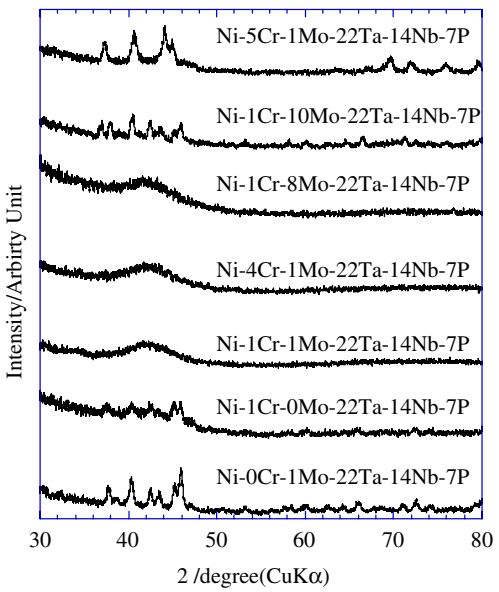

Fig. 1 X-ray diffraction patterns of copper-mold cast Ni–Cr–Mo–22Ta–14Nb–7P alloys of 1-mm diameter

14Nb–P alloys. The effects of chromium and molybdenum for formation of alloys composed of the amorphous single phase are slightly different. The maximum compositions to form the amorphous single phase are 4Cr–1Mo and 1Cr–8Mo in Ni–Cr–Mo–22Ta–14Nb–7P alloys. Further excess addition of chromium and molybdenum results in formation of heterogeneous alloys with nanocrystalline phases in the amorphous matrix. Unless both chromium and molybdenum were added, the alloys cannot be cast in the amorphous single phase.

Table 1 shows the corrosion rates of the alloys of 1-mm diameter estimated from the corrosion weight loss by immersion for 168 h in 6 and 12 M HCl at 30 °C. No detectable corrosion weight loss was observed for all alloys in 6 M HCl, indicating the fact that all these alloys have very high corrosion resistance. The corrosion rate measured in 12 M HCl is affected by the presence of the nanocrystalline phases. The Ni–Cr–Mo–22Ta–14Nb–7P alloys of the amorphous single phase did not show the corrosion weight loss in 12 M HCl, while all alloys consisting of nanocrystalline phases in the amorphous matrix show the detectable corrosion loss in 12 M HCl. The amorphous single phase is the prerequisite for undetectable corrosion loss in 12 M HCl.

There may be a tendency that the corrosion resistance of 4P alloys is slightly lower than that of 7P alloys. In spite of the amorphous single phase, the 1Cr–2Mo–4P and 2Cr–1Mo–4P alloys show the detectable corrosion loss, although the corrosion loss is significantly low. An interesting fact is that the 2Cr–2Mo–4P alloy did not show detectable corrosion weight loss. It can therefore be said that in the alloys composed of the amorphous single phase, the increase in both chromium and molybdenum enhances the corrosion resistance.

Figure 2 shows polarization curves of representative alloys measured in 6 M HCl. Reflecting the fact that these alloys are all immune to corrosion in 6 M HCl, these alloys are all spontaneously passive, and the open circuit potential is in the passive region of chromium. Although the corrosion weight loss could not be detected in 6 M HCl, the polarization curves show difference in the structures of the alloys. The alloys composed of the nanocrystalline phases in the amorphous matrix show higher anodic current density in comparison with the alloys of the amorphous single phase.

As shown in Fig. 3, among the alloys composed of the amorphous single phase, the 2Cr–1Mo alloy with the higher chromium content shows lower anodic current than the 1Cr–1Mo alloy with the lower chromium content. A slight increase in molybdenum content from the1Cr–1Mo alloy to the 1Cr–2Mo alloy is also effective in decreasing the anodic current density. Consequently, potentiodynamic polarization curves are more sensitive than the corrosion weight loss test, and the difference in corrosion loss with alloy structure and/or composition found in 12 M HCl has been detected in anodic polarization curves measured in 6 M HCl where the corrosion loss experiments could not detect the effect of difference in structure and/or composition.

For a better understanding of the superiority of the addition of three corrosion-resistant elements, that is, chromium, tantalum, and molybdenum, to the alloy, X-ray photoelectron spectroscopic analysis was performed for the specimens before and after immersion in 6 and 12 M HCl at 30 °C for 168 h. The P 2p spectrum consisted of two peaks, that is, the elemental state peak at 129.1 eV and the P^{5+} state peak at 133.7 eV, the latter of which corresponds to phosphorus in phosphate type anion. Because of the presence of oxygen-forming phosphate, the superposition of the O 1s spectra from PO_4^{3-}, O^{2-} and OH^- gave a single broad peak at about 531.3 eV. The metallic state peak of Ni $2p_{3/2}$ spectrum was observed at about 852.7 eV, but the oxidized state signal of nickel was not detected. The Cr $2p_{3/2}$ spectrum was composed of two peaks: the metallic state peak at about 573.2 eV and the Cr^{3+} state

Table 1 Corrosion rates of cast alloy rods of 1-mm diameter in concentrated hydrochloric acids

Alloy composition (at.%)	Structure	Corrosion rate (mm $year^{-1}$)	
		6 M HCl	12 M HCl
Ni–0Cr–1Mo–22Ta–14Nb–7P	Am + Xal	$<1.5\times10^{-4}$	7.2×10^{-4}
Ni–1Cr–0Mo–22Ta–14Nb–7P	Am + Xal	$<1.5\times10^{-4}$	3.5×10^{-4}
Ni–1Cr–1Mo–22Ta–14Nb–7P	Am	$<1.5\times10^{-4}$	$<1.5\times10^{-4}$
Ni–4Cr–1Mo–22Ta–14Nb–7P	Am	$<1.5\times10^{-4}$	$<1.5\times10^{-4}$
Ni–1Cr–8Mo–22Ta–14Nb–7P	Am	$<1.5\times10^{-4}$	$<1.5\times10^{-4}$
Ni–5Cr–1Mo–22Ta–14Nb–7P	Am + Xal	$<1.5\times10^{-4}$	5.3×10^{-4}
Ni–1Cr–10Mo–22Ta–14Nb–7P	Am + Xal	$<1.5\times10^{-4}$	5.3×10^{-4}
Ni–1Cr–2Mo–22Ta–14Nb–4P	Am	$<1.5\times10^{-4}$	2.0×10^{-4}
Ni–2Cr–1Mo–22Ta–14Nb–4P	Am	$<1.5\times10^{-4}$	1.7×10^{-4}
Ni–2Cr–2Mo–22Ta–14Nb–4P	Am	$<1.5\times10^{-4}$	$<1.5\times10^{-4}$

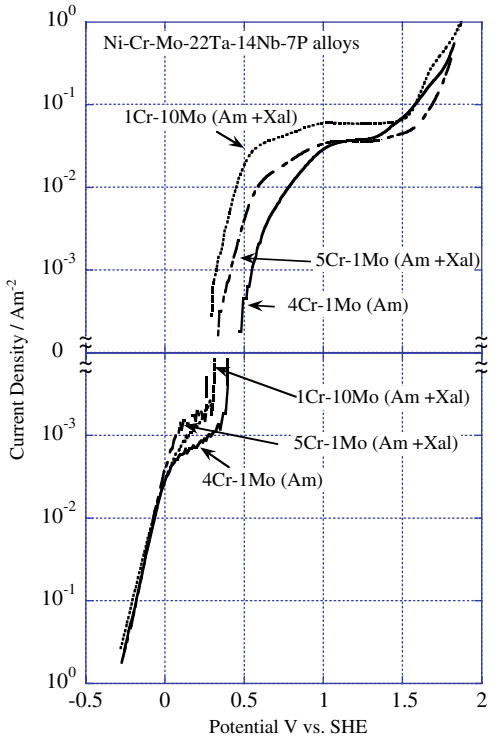

Fig. 2 Potentiodynamic polarization curves of copper-mold cast Ni–Cr–Mo–22Ta–14Nb–7P alloys of 1-mm diameter

peak at about 577.6 eV, although the metallic state peak for these alloys covered with the surface film was very weak. The Ta $4f_{7/2}$ and $4f_{5/2}$ spectra consisted of two doublets: the Ta $4f_{7/2}$ and $4f_{5/2}$ peaks corresponding to the metallic Ta^0 state were located at about 22.7 and 24.5 eV, respectively, and those corresponding to the Ta^{5+} state appeared at about 26.5 and 28.4 eV, respectively.

Since the alloys contain both molybdenum and tantalum, the most intense peaks of molybdenum, Mo 3d peaks, were superposed upon the Ta $4d_{5/2}$ peak. Accordingly, the real Mo 3d spectrum was estimated by subtracting the Ta $4d_{5/2}$ spectrum from the observed spectrum. The intensities of the Ta^0 and Ta^{5+} $4d_{5/2}$ spectra were estimated from those of the Ta^0 and Ta^{5+} 4f spectra. For this purpose, the standard Ta^0 and Ta^{5+} $4d_{5/2}$ spectra and the peak intensity ratios of Ta^0 $4d_{5/2}/Ta^0$ $4f_{7/2}$ and Ta^{5+} $4d_{5/2}/Ta^{5+}$ $4f_{7/2}$ were obtained from Ta metal and Ta_2O_5 formed by thermal oxidation of tantalum. The peaks of the Ta^0 and Ta^{5+} $4d_{5/2}$ spectra of Ta metal and Ta_2O_5 appeared at about 227.5 and 231.3 eV. After subtraction of the Ta $4d_{5/2}$ spectra, the remaining spectrum was separated in four doublets of molybdenum. The binding energies of the Mo $3d_{5/2}$ electrons in Mo^0, Mo^{4+}, Mo^{5+}, and Mo^{6+} states were taken as 227.8, 228.8, 230.3, and 232.4 eV, respectively.

Quantitative determination of the thickness and composition of the surface film and the composition of the underlying alloy surface was performed after integrated intensities were obtained separately for the metallic and oxidized states in addition to integrated intensities of O 1s and C 1s spectra. Figure 4 shows examples of the analytical results for the spontaneously passivated alloy by X-ray photoelectron spectroscopy. The most important characteristic is that the surface film composition was not largely changed before and after immersion. Before immersion, all specimens were polished in cyclohexane with silicon carbide paper up to no. 1500, degreased in acetone and dried in air. Therefore, before immersion, the mechanically polished specimens had been covered with the air-formed film, and because of high protectiveness of the air-formed film, spontaneous passivation occurred in aggressive hydrochloric acids.

The surface films are rich in tantalum, chromium, and niobium, and the comparison of the film composition with the alloy composition reveals particular enrichment of

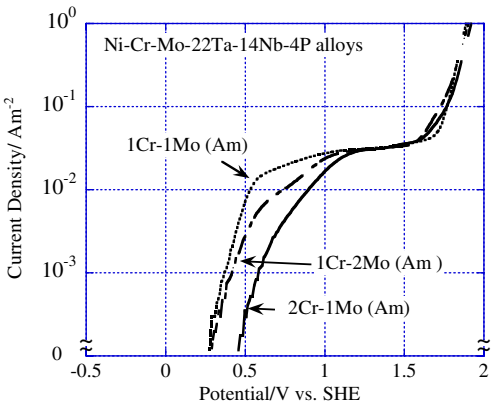

Fig. 3 Potentiodynamic anodic polarization curves of copper-mold cast amorphous Ni–Cr–Mo–22Ta–14Nb–4P alloys of 1-mm diameter

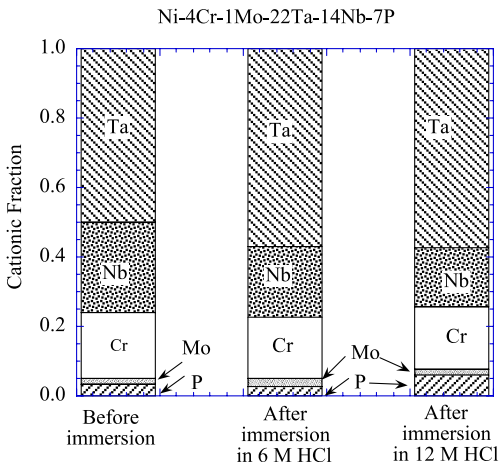

Fig. 4 Compositions of surface films on copper-mold cast amorphous Ni–4Cr–1Mo–22Ta–14Nb–7P alloy of 1-mm diameter before and after immersion in 6 and 12 M HCl for 168

chromium. The high chromium content of the film is responsible for the high corrosion resistance even in 12 M HCl. Some oxidized molybdenum and phosphorus are also found in the film.

As shown in Fig. 5, another characteristic is the decrease in the chromium content of the film on the heterogeneous alloys by immersion in 12 M HCl. The heterogeneity may prevent maintaining the sufficient chromium content for corrosion resistance in 12 M HCl.

Figure 6 shows the weight of molybdenum contained in the passive film. The molybdenum metal is passive around the open circuit potentials of these alloys, forming tetravalent molybdenum oxide film such as MoO_2 [23]. However, air exposure of passive molybdenum metal is known to be oxidized to hexavalent molybdenum in the outer part of the passive film. As shown in Fig. 6, tetravalent molybdenum is formed by air exposure possibly in the inner part of the film, and immersion in aggressive hydrochloric acids tends to increase the weight of tetravalent molybdenum, suggesting that the corrosion resistance in the aggressive acids is provided by the increase in the tetravalent molybdenum content of the film. On the other hand, as shown in Fig. 7, in the heterogeneous alloy, the molybdenum content decreases by immersion in the aggressive acids, suggesting the degradation of the protectiveness of the air-formed film by immersion in the acids. In other words, spontaneously passive alloys with high corrosion resistance can be characterized by their ability to improve the protectiveness spontaneously by immersion in the aggressive acids.

In relation to the roles of corrosion-resistant elements, the angle-resolved XPS examination gave the useful information. Figure 8 shows the change in the results of composition analysis by the change in the incidence angle

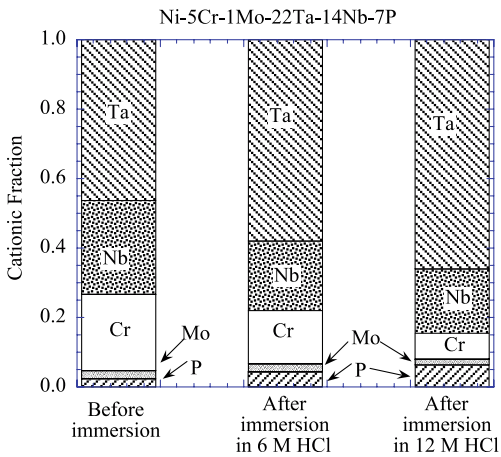

Fig. 5 Compositions of surface films on copper-mold cast Ni–5Cr–1Mo–22Ta–14Nb–7P alloy of 1-mm diameter before and after immersion in 6 and 12 M HCl for 168

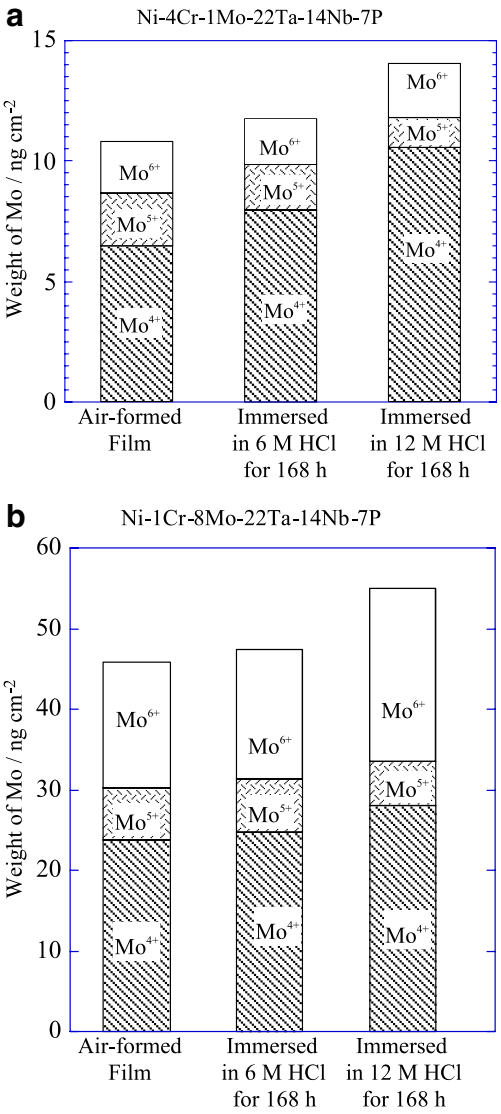

Fig. 6 Weights of molybdenum species in the surface films on copper-mold cast amorphous Ni–4Cr–1Mo–22Ta–14Nb–7P (**a**) and Ni–1Cr–8Mo–22Ta–14Nb–7P (**b**) alloys of 1-mm diameter before and after immersion in 6 and 12 M HCl for 168

of X-ray for XPS. In the measurement at the high incidence angle, the signals from the inner part of film are intensified. Thus, the result shown in Fig. 8 suggests that chromium and molybdenum are rich in the inner part of the film.

Discussion

Hashimoto and his coworkers studied the corrosion behavior of binary Cr-valve metal [24–26], Mo-valve metal [27–30], and Cr–Mo [31] alloys prepared by sputter deposition in concentrated hydrochloric acids. These alloys were all composed of a single phase solid solution. They had higher corrosion resistance in concentrated hydro-

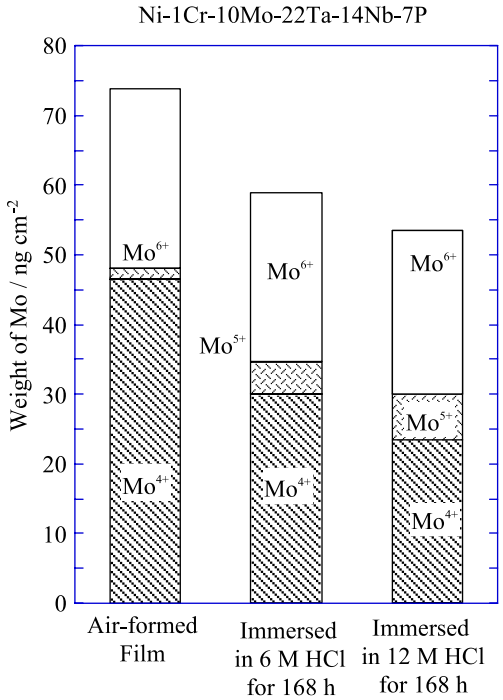

Fig. 7 Weights of molybdenum species in the surface films on copper-mold cast Ni–1Cr–10Mo–22Ta–14Nb–7P alloy of 1-mm diameter before and after immersion in 6 and 12 M HCl for 168

chloric acids than alloy component metals and passivated spontaneously because of the high protectiveness and stability of the air-formed film.

The surface films formed on binary Cr-valve metal alloys were not the heterogeneous mixture of chromium oxyhydroxide and valve metal oxyhydroxide but the double oxyhydroxide, such as $Cr_{1-x}Ta_xO_y(OH)_{3+2x-2y}$, in which the electronic interaction was found between Cr^{3+} and Ta^{5+} [32]. Because the corrosion resistance of the binary Cr–Ta alloys was significantly higher than chromium and tantalum metals in concentrated hydrochloric acids, the passive $Cr_{1-x}Ta_xO_y(OH)_{3+2x-2y}$ film was definitely more stable and protective in comparison with the passive chromium oxyhydroxide and tantalum oxyhydroxide films. On the other hand, the surface films on Cr–Mo and Mo-valve metal alloys consisted of bilayer structure of the outer valve metal or chromium oxyhydroxide and the inner tetravalent molybdenum oxide, and the corrosion resistance of the binary alloys was better than alloy component metals in concentrated hydrochloric acids.

In the present study, total amounts of less than a few atomic percent additions of both chromium and molybdenum were effective in enhancing the corrosion resistance, and only 1 at.% increase in chromium or molybdenum content was required for undetectable corrosion loss in 12 M HCl. Thus, the presence of sufficient amounts of both chromium and molybdenum even in small amounts is prerequisite for undetectable corrosion loss in 12 M HCl. XPS analysis showed that chromium, tantalum, and niobium were significantly concentrated in the film, and chromium and molybdenum were apt to be rich in the inner part of film. Although chromium is rich in the inner part of film, the stability of the film formed on Ni–Cr–Mo–22Ta–14Nb–7P alloys in this experiment is higher than those formed on tantalum, niobium, and chromium metals [32]. In particular, the corrosion resistance of niobium is significantly lower than that of tantalum. Consequently, the present results suggests the formation of the triple $Cr_{1-x-y}Ta_xNb_yO_z(OH)_{3+2x+2y-2z}$ oxyhydroxide film having higher stability than the films formed on corrosion-resistant single metals. When the alloys were exposed to air after mechanical polishing in cyclohexane, tantalum, niobium, and chromium having a high affinity to oxygen should be preferentially oxidized, possibly forming the triple $Cr_{1-x-y}Ta_xNb_yO_z(OH)_{3+2x+2y-2z}$ oxyhydroxide film. Among these three elements, the affinity of tantalum and niobium to oxygen is higher than chromium, and hence, the chromium content in the film may be higher in the inner part of the film. At ambient temperature, the outward diffusion of tantalum, niobium, and chromium through the underlying alloy to the film/alloy interface is slow, and hence, preferential oxidation of chromium and valve metals gives rise to the deficiency of chromium, tantalum, and niobium at the film/alloy interface. This leads to an enrichment of molybdenum and an increase in oxygen potential at the film/alloy interface, with a consequent formation of the inner tetravalent molybdenum oxide layer.

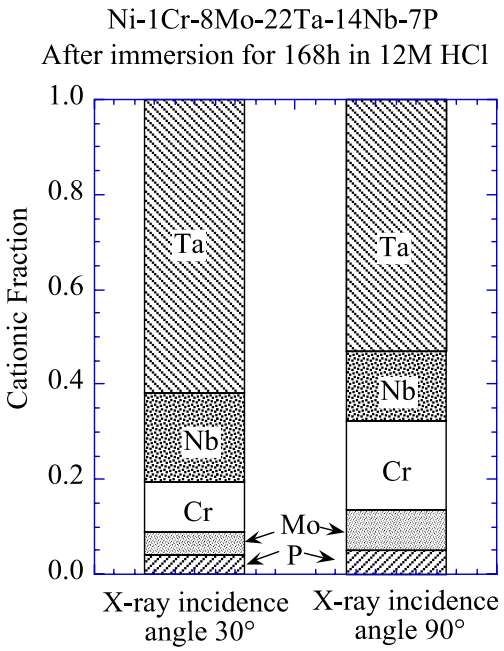

Fig. 8 Analytical results of the spontaneously passive film on copper-mold cast amorphous Ni–1Cr–8Mo–22Ta–14Nb–7P alloy of 1-mm diameter after immersion in 12 M HCl for 168 measured changing the incidence angle of X-ray in XPS at 30° and 90°

The open circuit potentials of these alloys are higher than the transpassive potential of molybdenum. Thus, if molybdenum is directly exposed to the solution, transpassive dissolution of molybdenum occurs. By contrast, the inner tetravalent molybdenum oxide is well protected by the outer triple oxyhydroxide film and acts as the more effective barrier against diffusion of matters through the film.

Conclusions

Amorphous bulk Ni–Cr–Mo–22Ta–14Nb–P alloys with spontaneous passivity in concentrated hydrochloric acids were prepared by copper-mold casting. Ni–(1–4)Cr–1Mo–22Ta–14Nb–7P and Ni–1Cr–(1–8)Mo–22Ta–14Nb–7P alloys were composed of an amorphous single phase, and their corrosion weight loss was not detected after immersion for 168 h in 12 M HCl.

Potentiodynamic anodic polarization is more sensitive, and an increase in 1 at.% chromium or molybdenum in the Ni–1Cr–1Mo–22Ta–14Nb–4P alloy composed of the amorphous single phase decreased the anodic current measured in 6 M HCl.

XPS analysis revealed significant enrichment of chromium, tantalum, and niobium in the film and enrichment of chromium and molybdenum in the inner part of the film.

The high corrosion resistance and spontaneous passivity of these alloys were interpreted in terms of the formation of highly stable outer triple oxyhydroxide $Cr_{1-x-y}Ta_xNb_yO_z(OH)_{3+2x+2y-2z}$ film and the inner MoO_2 layer effective as the barrier for diffusion of matters through the film.

References

1. Naka N, Hashimoto K, Masumoto T (1974) J Inst Metals 38:835
2. Inoue A, Ohtera K, Kita K, Masumoto T (1988) Mater Jpn J Appl Phys 27:L2248
3. Inoue A, Zhang T, Masumoto T (1989) Mater Trans JIM 30:965
4. Kato A, Suganuma T, Horikiri H, Kawamura Y, Inoue A, Masumoto T (1994) Mater Sci Eng A179–A180:112
5. Kawamura Y, Kato H, Inoue A, Masumoto T (1995) Appl Phys Lett 67:2008
6. Inoue A, Gook JS (1995) Mater Trans JIM 36:1180
7. Inoue A (1999) Mater Sci Eng A267:171
8. Habazaki H, Naruse Y, Konno K, Ukai H, Izumiya K, Hashimoto K (2001) Corrosion and corrosion protection. In: Sinclair JD, Kalman E, Kendig MW, Plieth W, Smyrl WH (eds) The Electrochemical Society PV 2001-22. The Electrochemical Society Proceedings Series. Pennington, NJ, pp 130–137
9. Habazaki H, Sato T, Kawashima A, Asami K, Hashimoto K (2001) Mater Sci Eng A304–306:696
10. Kawashima A, Habazaki H, Hashimoto K (2001) Mater Sci Eng A304–306:753
11. Habazaki H, Ukai H, Izumiya K, Hashimoto K (2001) Mater Sci Eng A 318:77
12. Katagiri H, Meguro S, Yamasaki M, Habazaki H, Sato T, Kawashima A, Asami K, Hashimoto K (2001) Corros Sci 43:183
13. Shinomiya H, Nakazawa A, Kato Z, El-Moneim AA, Niizeki Y, Asami K, Hashimoto K (2006) Corrosion and electrochemistry of advanced materials. In: NacDougall B, Fujimoto S, Habazaki H, Akiyama E (eds) The Electrochemical Society PV 2006-, The Electrochemical Society Proceedings Series, Pennington, NJ, pp 49–59
14. Asami K (1976) J Electron Spectrosc 9:469
15. Asami K, Hashimoto K (1977) Corros Sci 17:559
16. Asami K, Hashimoto K, Shimodaira S (1977) Corros Sci 17:713
17. Asami K, Hashimoto K (1984) Corros Sci 24:83
18. Akiyama E, Habazaki H, Kawashima A, Asami K, Hashimoto K (1994) Mater Sci Eng A181–182:1128
19. Teramoto K, Asami K, Hashimoto K (1978) Corros Eng 27:57
20. Kim KH, Yoshioka H, Habazaki H, Kawashima A, Asami K, Hashimoto K (1992) Corros Sci 33:1507
21. Yoshioka H, Yan Q, Kawashima A, Asami K, Hashimoto K (1990) Corros Sci 31:349
22. Hashimoto K, Kasaya M, Asami K, Masumoto T (1977) Corros Eng 26:445
23. Habazaki H, Kawashima A, Asami K, Hashimoto K (1992) Corros Sci 33:225
24. Kim JH, Akiyama E, Yoshioka H, Habazaki H, Kawashima A, Asami K, Hashimoto K (1993) Corros Sci 34:975
25. Kim JH, Akiyama E, Habazaki H, Kawashima A, Asami K, Hashimoto K (1993) Corros Sci 34:1817
26. Kim JH, Akiyama E, Habazaki H, Kawashima A, Asami K, Hashimoto K (1993) Corros Sci 34:1947
27. Park PY, Akiyama E, Habazaki H, Kawashima A, Asami K, Hashimoto K (1995) Corros Sci 37:307
28. Park PY, Akiyama E, Kawashima A, Asami K, Hashimoto K (1996) Corros Sci 38:397
29. Park PY, Akiyama E, Habazaki H, Kawashima A, Asami K, Hashimoto K (1996) Corros Sci 38:1649
30. Park PY, Akiyama E, Habazaki H, Kawashima A, Asami K, Hashimoto K (1996) Corros Sci 38:1731
31. Park PY, Akiyama E, Kawashima A, Asami K, Hashimoto K (1995) Corros Sci 37:1843
32. Kim JH, Akiyama E, Habazaki H, Kawashima A, Asami K, Hashimoto K (1994) Corros Sci 36:511